Electronic Supplementary Material (ESI) for Nanoscale.

Electronic Supplementary Information

Top-down synthesis of single layered $Cs_4CuSb_2Cl_{12}$ halide perovskite nanocrystals for photoelectrochemical application

Xu-Dong Wang,[†] Nai-Hua Miao,[†] Jin-Feng Liao, Wen-Qian Li, Yao Xie, Jian Chen, Zhi-Mei Sun, Hong-Yan Chen, and Dai-Bin Kuang*[a]

[†]Xu-Dong Wang and Nai-Hua Miao contributed equally.

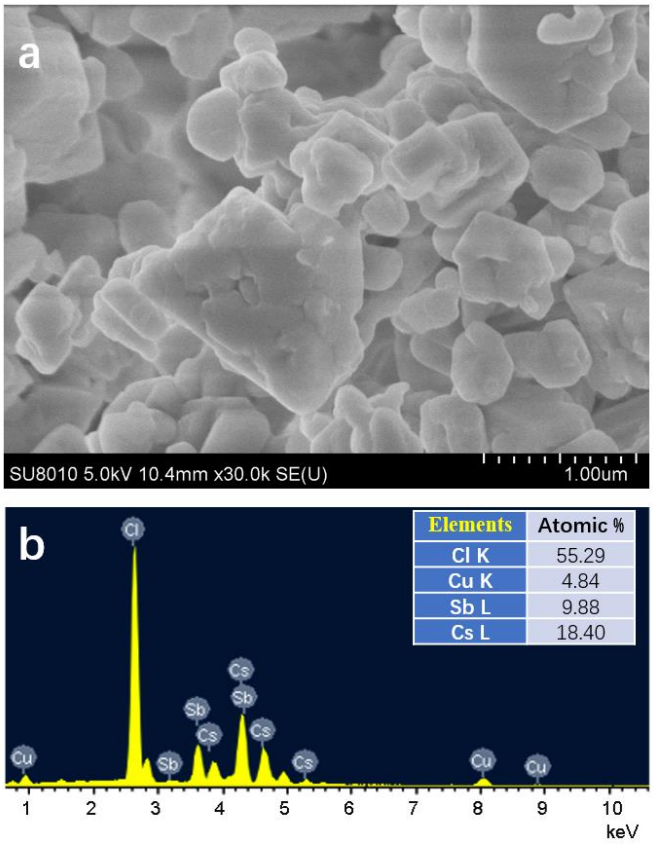

Fig. S1 SEM image (a) and EDX spectrum (b) of the $Cs_4CuSb_2Cl_{12}$ microcrystals.

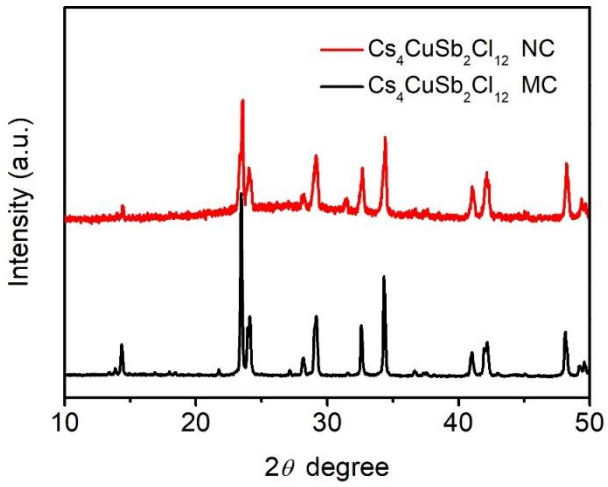

Fig. S2 XRD patterns of $Cs_4CuSb_2Cl_{12}$ NCs and microcrystals.

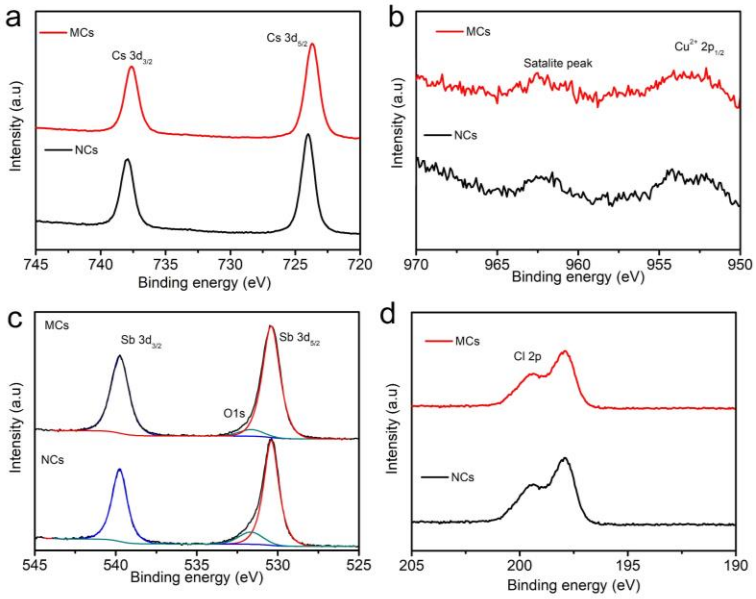

Fig. S3 XPS spectra of $Cs_4CuSb_2Cl_{12}$ before and after ultrasonic exfoliation: (a) Cs, (b) Cu, (c) Sb and (d) Cl.

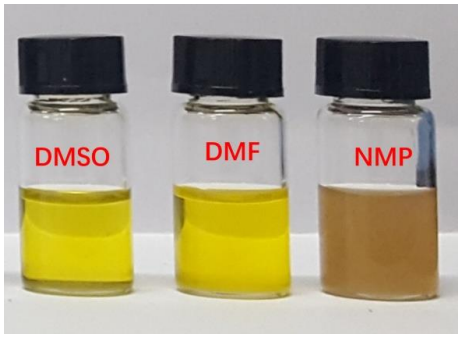

Fig. S4 Photographs of ultrasonic exfoliation $Cs_4CuSb_2Cl_{12}$ microcrystal in DMSO, DMF and NMP.

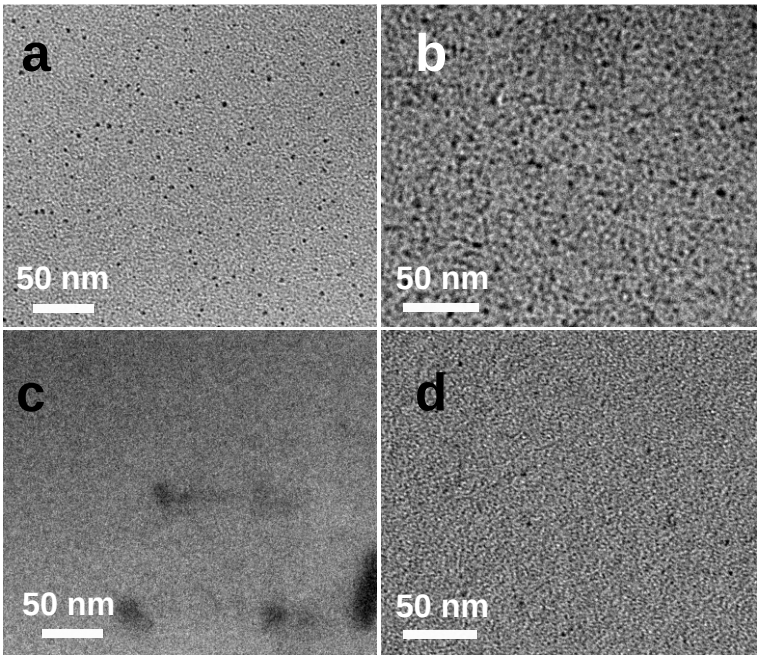

Fig. S5 TEM images of ultrasonic exfoliation $Cs_4CuSb_2Cl_{12}$ nanocrystal in different solvents: (a) Toluene, (b) CCl_4, (c) Ethyl acetate, (d) Hexane.

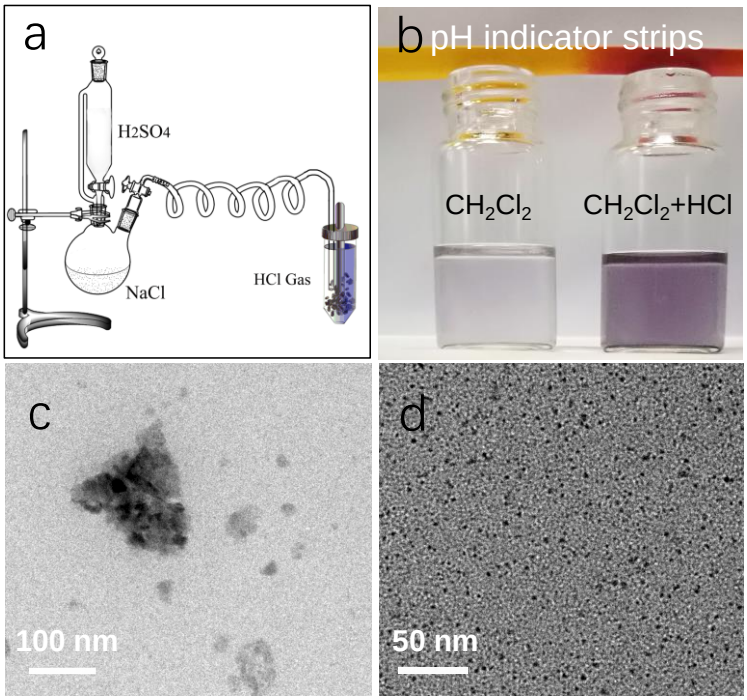

Fig. S6 (a) Schematic illustration of HCl assisted ultrasonic exfoliation in CH_2Cl_2. (b) Photographs of liquid-phase exfoliation with and without HCl. TEM image of $Cs_4CuSb_2Cl_{12}$ nanocrystals in CH_2Cl_2 without HCl (c) and with HCl (d) after sonication and centrifugation with 500 rpm.

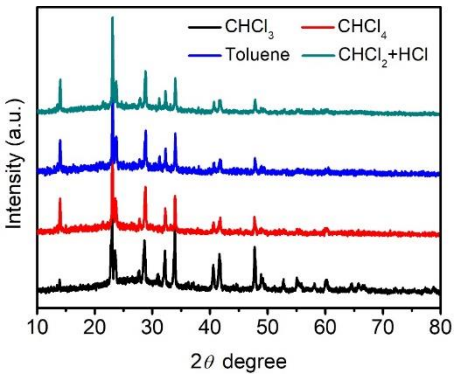

Fig. S7 XRD patterns of $Cs_4CuSb_2Cl_{12}$ NCs obtained using different solvents ($CHCl_3$, CCl_4, toluene) and by HCl assisted ultrasonic exfoliation in CH_2Cl_2.

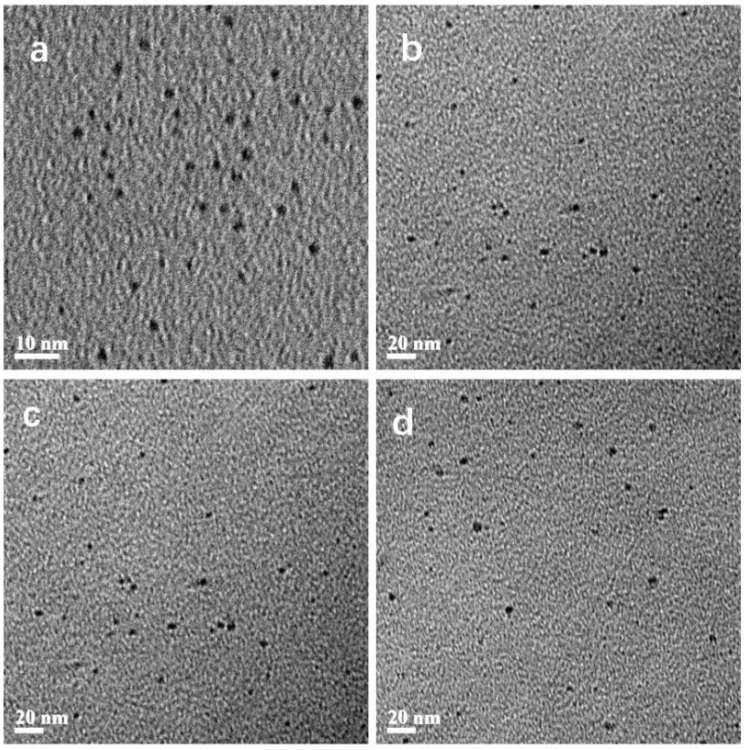

Fig. S8 TEM images of $Cs_4CuSb_2Cl_{12}$ nanocrystals ultrasonic exfoliation in $CHCl_3$ after centrifugation under different speeds: (a) 500 rpm, (b) 1000 rpm, (c) 2000 rpm, (d) 4000 rpm.

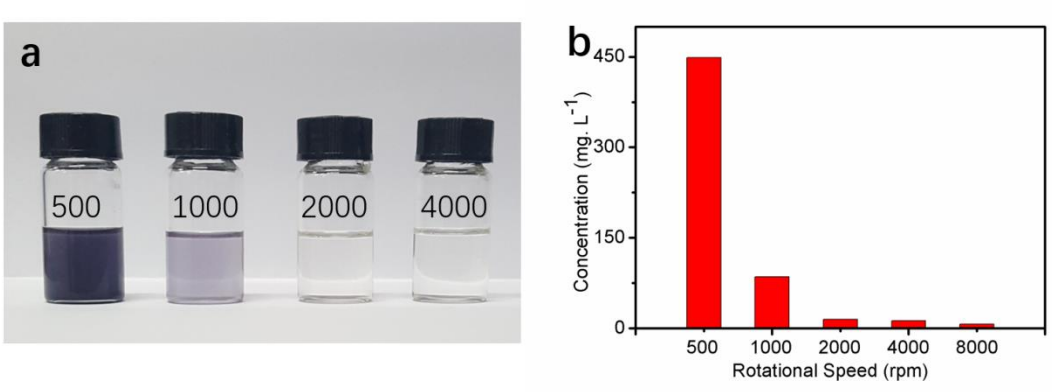

Fig. S9 Photograph (a) and concentration (b) of $Cs_4CuSb_2Cl_{12}$ nanocrystals in $CHCl_3$ prepared after ultrasonication and centrifugation with different speeds.

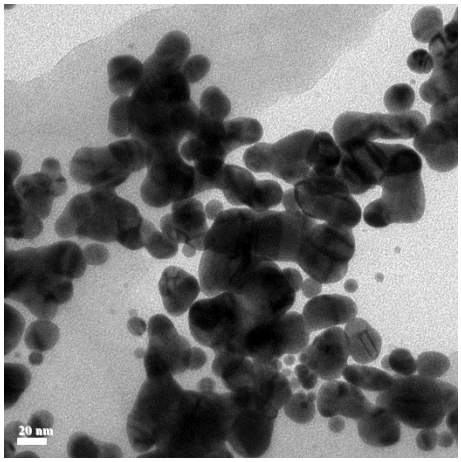

Fig. S10 $Cs_4CuSb_2Cl_{12}$ NCs prepared by ultrasonication in $CHCl_3$ without OA.

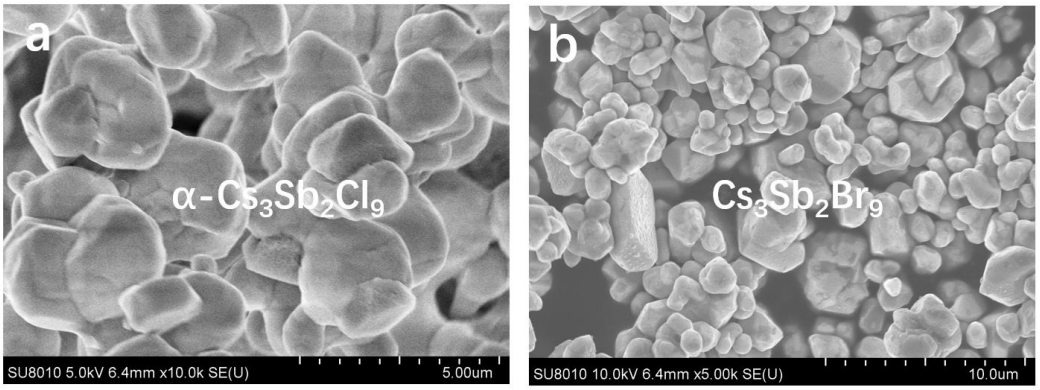

Fig. S11 XRD patterns of the $Cs_3Sb_2Cl_9$ (a) microcrystals and $Cs_3Sb_2Br_9$ (b) microcrystals.

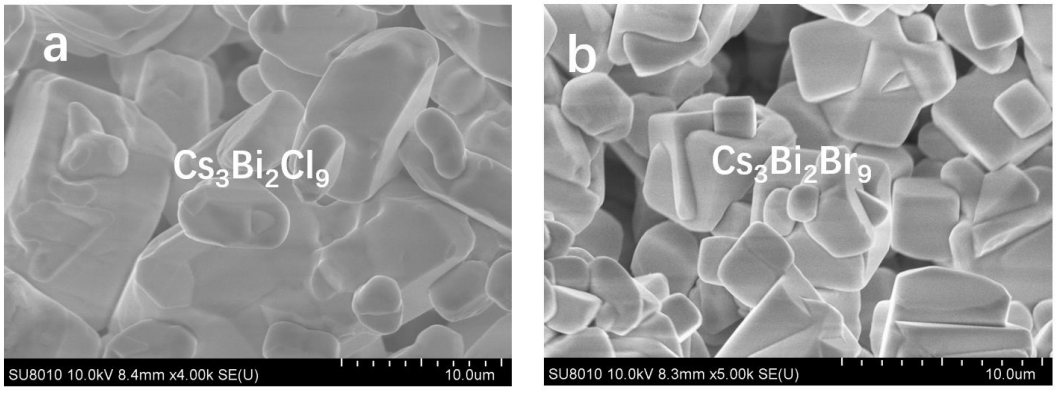

Fig. S12 XRD patterns of the $Cs_3Bi_2Cl_9$ (a) microcrystals and $Cs_3Bi_2Br_9$ (b) microcrystals.

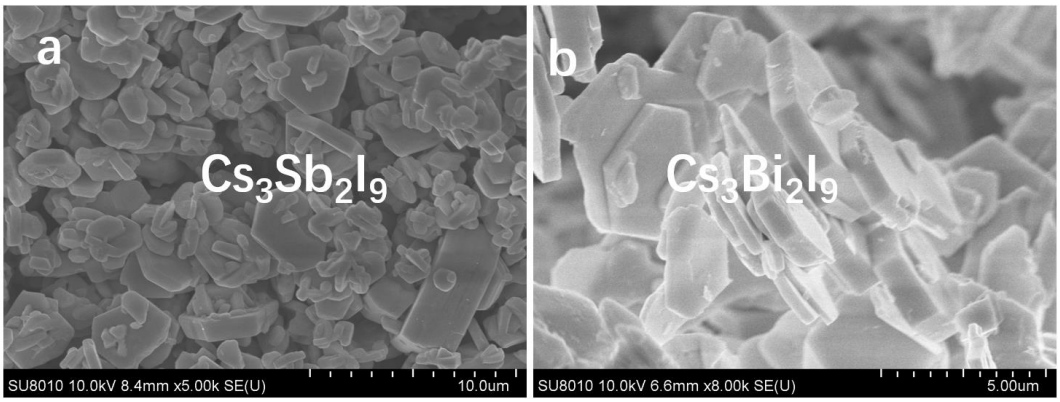

Fig. S13 XRD patterns of the $Cs_3Sb_2I_9$ (a) microcrystals and $Cs_3Bi_2I_9$ (b) microcrystals.

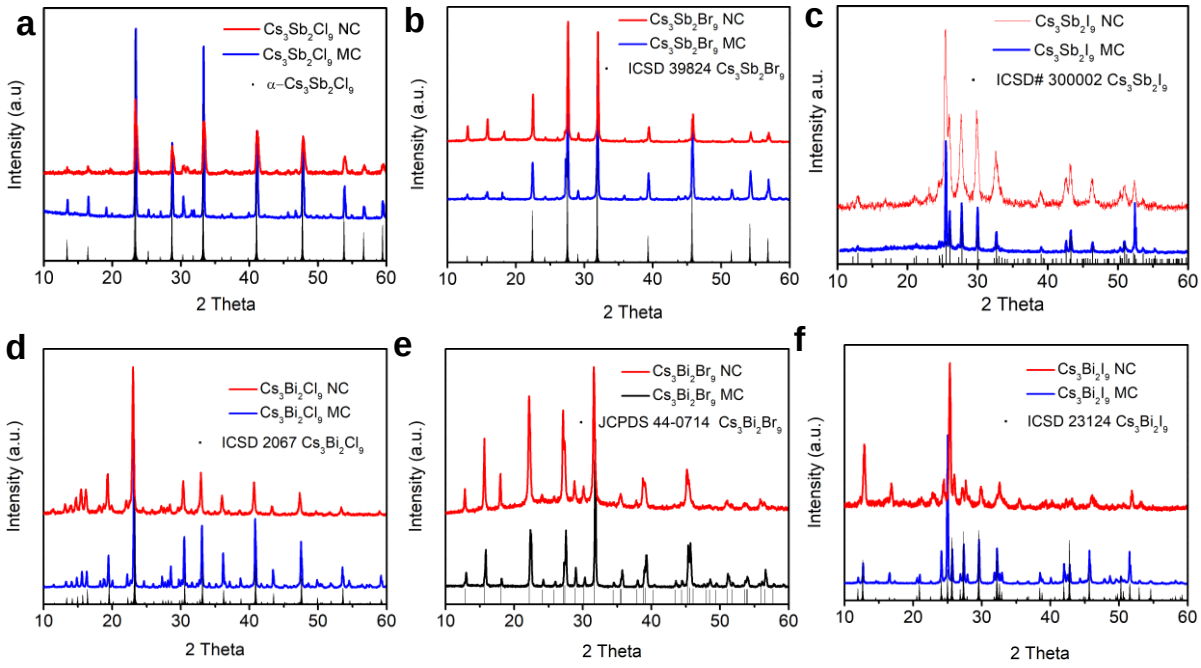

Fig. S14 The XRD patterns of $Cs_3Sb_2X_9$ and $Cs_3Bi_2X_9$ before and after exfoliation. (The XRD patterns of the as-prepared $Cs_3Sb_2Cl_9$ matches with the α-$Cs_3Sb_2Cl_9$ phase. Other peaks are assigned to a secondary phase (No. ICSD 2066).)

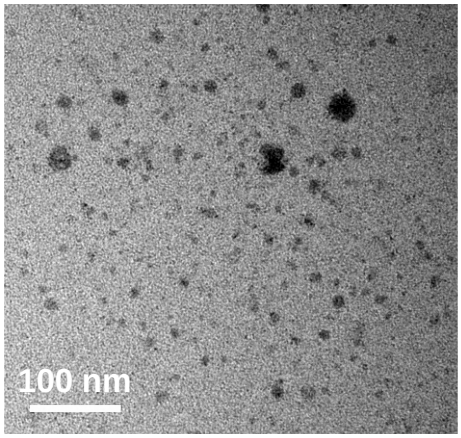

Fig. S15 $Cs_3Sb_2Cl_9$ NCs in $CHCl_3$ after sonication 60 min and centrifugation at 500 rpm.

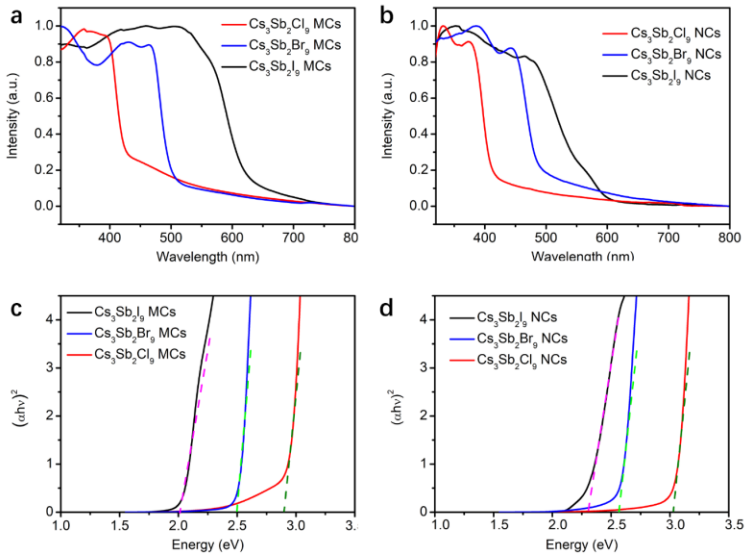

Fig. S16 UV-Vis spectra of $Cs_3Sb_2X_9$ microcrystals (a) and NCs (b); (c, d) corresponding Tauc plots.

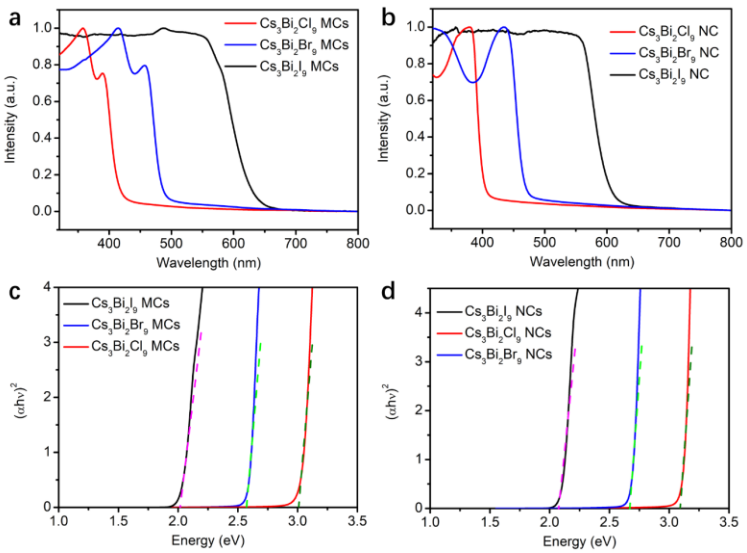

Fig. S17 UV-Vis spectra of $Cs_3Bi_2X_9$ microcrystals (a) and NCs (b); (c, d) corresponding Tauc plots.

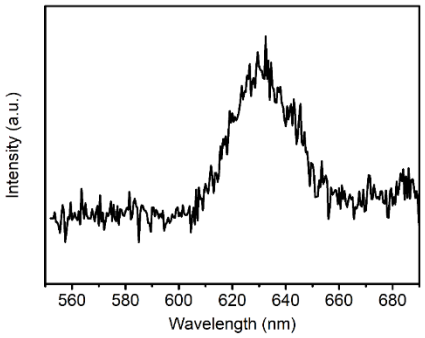

Fig. S18 Photoluminescence spectra of the $Cs_4CuSb_2Cl_{12}$ NCs.

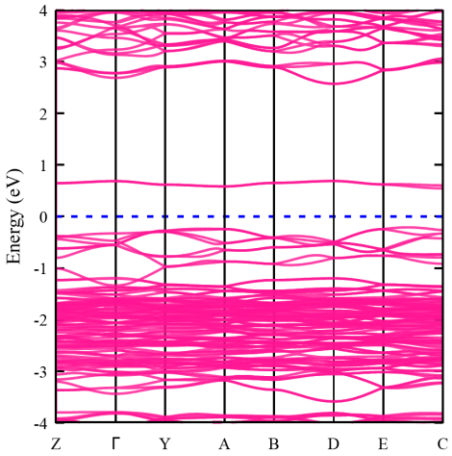

Fig. S19 Electronic band structures of the bulk $Cs_4CuSb_2Cl_{12}$.

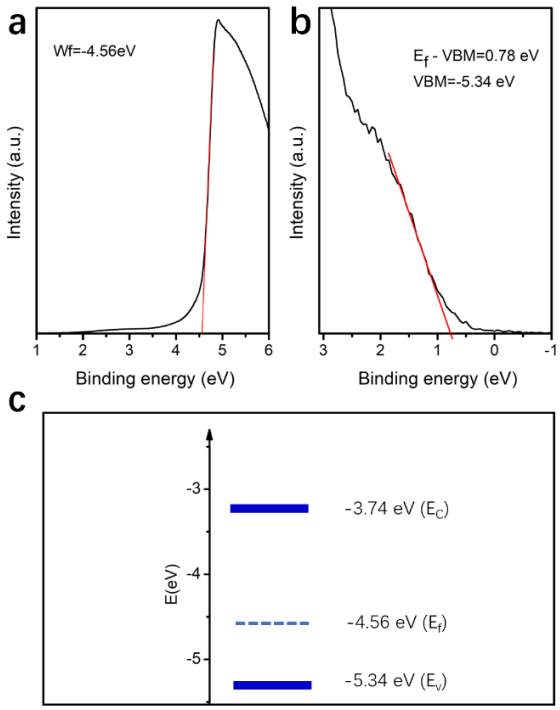

Fig. S20 (a, b) UPS characteristics of $Cs_4CuSb_2Cl_{12}$ NCs film, (c) Schematic diagram of the band structure for $Cs_4CuSb_2Cl_{12}$ NCs.

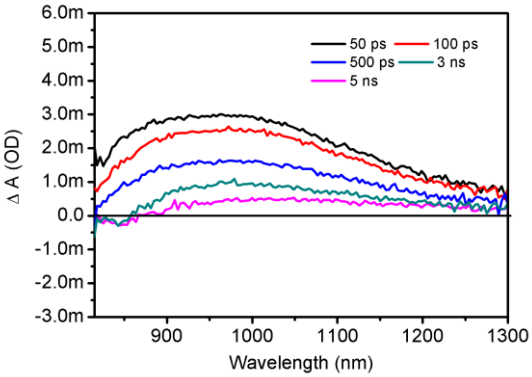

Fig. S21 TA spectra at infrared region indicated delay time from 50 ps to 5 ns.

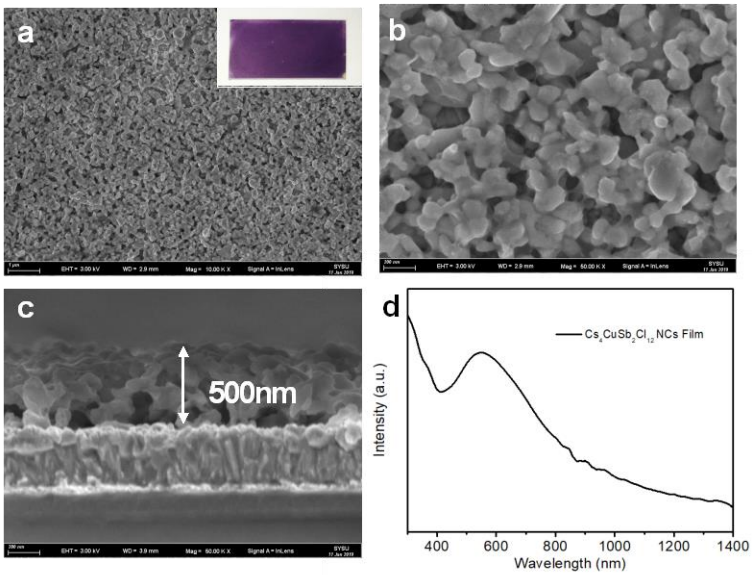

Fig. S22 SEM images (a-c) and inset, a photograph of $Cs_4CuSb_2Cl_{12}$ NCs deposited on the FTO, (d) UV-Vis-NIR spectra of the of $Cs_4CuSb_2Cl_{12}$ film.

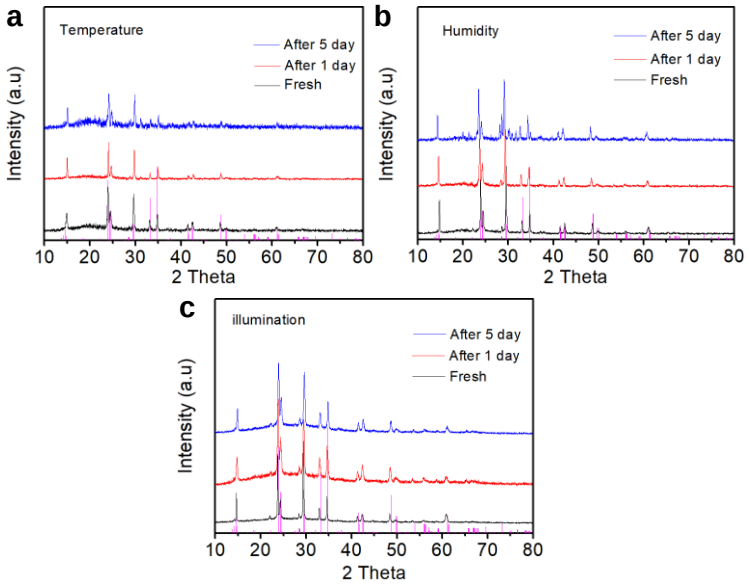

Fig. S23 Stability tests of $Cs_4CuSb_2Cl_{12}$ NCs: (a) heating at 80 ℃ (b) exposing to humidity of 65%, and (c) illumination at 100 $mWcm^{-2}$.

Table S1. Experimental and calculated structural parameters and bandgap of bulk $Cs_3Sb_2Cl_9$, $Cs_3Sb_2Br_9$, $Cs_3Sb_2I_9$ and $Cs4CuSb_2Cl_{12}$.

		$Cs_3Sb_2Cl_9$		$Cs_3Sb_2Br_9$		$Cs_3Sb_2I_9$		$Cs_4CuSb_2Cl_{12}$	
		GGA PBE	Expt.	GGA PBE	Expt.	GGA PBE	Expt.	GGA PBE	Expt.
	a (Å)	7.645	7.610	7.976	7.930	8.458	8.348	13.175	13.026
	b (Å)	7.645	7.610	7.976	7.930	8.458	8.348	7.349	7.327
	c (Å)	9.370	9.320	9.820	9.716	21.268	20.928	13.161	13.006
	a (°)	90.00	90.00	90.00	90.00	90.00	90.00	90.00	90.00
	β (°)	90.00	90.00	90.00	90.00	90.00	90.00	112.36	111.98
PBE	E_g(eV)	2.42	2.91	1.90	2.51	1.73	2.02	0	1.02
HSE06 (PBE+U)	E_g(eV)	3.03	-	2.52	-	2.30	-	0.48 (0.80)	-

Table S2. Experimental and calculated structural parameters and bandgap of monolayer $Cs_3Sb_2Cl_9$, $Cs_3Sb_2Br_9$, $Cs_3Sb_2I_9$ and $Cs4CuSb_2Cl_{12}$.

		$Cs_3Sb_2Cl_9$	$Cs_3Sb_2Br_9$	$Cs_3Sb_2I_9$	$Cs_4CuSb_2Cl_{12}$
	a (Å)	7.594	7.935	8.444	13.167
	b (Å)	7.594	7.935	8.444	7.315
PBE	E_g(eV)	2.72	2.27	2.08	2.01
HSE06(PBE+U)	E_g(eV)	3.47	2.93	2.61	0.68(0.91)
Expt.	E_g(eV)	3.05	2.58	2.30	1.6

Please note that: Usually, the HSE06 functional could well reproduce the experimental band gap of most compounds as shown in Table S1, except for the gap of $Cs_4CuSb_2Cl_{12}$ which is greatly underestimated. While the GGA-PBE underestimates all the gaps or even gives wrong value as often observed in the Cu-based compounds. [1-3] Therefore, in order to better reproduce the experimental electronic band gap of the bulk and single-layer $Cs_4CuSb_2Cl_{12}$, the GGA+U approach, which shows better agreement with our experiments, has been adopted for the electronic band structure and density of states.

References

1 M. Heinemann, B. Eifert, C. Heiliger, Phys. Rev. B: Condens. *Matter Mater. Phys.,* 2013, **87**, 115111.

2 R. Laskowski, P. Blaha, K. Schwarz, Phys. Rev. B: Condens. *Matter Mater. Phys.,* 2003, **67**, 075102.

3 M. Nolan, S. D. Elliott, *Phys. Chem. Chem. Phys*., 2006, **8**, 5350.